Journal of Energy Storage 62 (2023) 106762

Contents lists available at ScienceDirect

Journal of Energy Storage

journal homepage: www.elsevier.com/locate/est

Research Papers

Investigating the effect of size and number of layers of iron nanochannel on the thermal behavior and phase change process of calcium chloride/sodium sulfate hexa-hydrate with molecular dynamics simulation

Yun Xiang Zhang [a,b,c,d,e,f,*], As'ad Alizadeh [g], Azher M. Abed [h], Navid Nasajpour-Esfahani [i], Ghassan Fadhil Smaisim [j,k], Salema K. Hadrawi [l,m], Hussein Zekri [n,o], Shaghayegh Baghaei [p,**], Shadi Esmaeili [r], Meng Xia Wang [a,b,c,d,e,q,*]

[a] Nanchang Institute of Technology, 330000, China
[b] Hainan Vocational University of Science and Technology, 571126, China
[c] Shenzhen High-level Talents Development Promotion Association, 518000, China
[d] CDA International Accelerator, 999038, Poland
[e] Jiangxi Engineers Association, 330046, China
[f] University of Cyprus, 999058, Cyprus
[g] Department of Civil Engineering, College of Engineering, Cihan University-Erbil, Erbil, Iraq
[h] Air Conditioning and Refrigeration Techniques Engineering Department, Al-Mustaqbal University College, Babylon 51001, Iraq
[i] Georgia Institute of Technology, Department of Material Science and Engineering, 771 Ferst Dr NW, Atlanta, GA 30332, United States
[j] Department of Mechanical Engineering, Faculty of Engineering, University of Kufa, Iraq
[k] Nanotechnology and Advanced Materials Research Unit (NAMRU), Faculty of Engineering, University of Kufa, Iraq
[l] Refrigeration and Air-conditioning Technical Engineering Department, College of Technical Engineering, The Islamic University, Najaf, Iraq
[m] Computer Engineering Department, Imam Reza University, Mashhad, Iran
[n] College of Engineering, The American University of Kurdistan, Duhok, Kurdistan Region, Iraq
[o] Department of Mechanical Engineering, College of Engineering, University of Zakho, Zakho, Kurdistan Region, Iraq
[p] Department of Mechanical Engineering, Khomeinishahr Branch, Islamic Azad University, Khomeinishahr, Iran
[q] University of Wollongong, 999029, Australia
[r] Department of Physics, Semnan University, Semnan, Iran

ARTICLE INFO

Keywords:
Phase change material (PCM)
Thermal behavior
Heat flux
Charge time
Discharge time
Molecular dynamics simulation

ABSTRACT

Phase change material (PCM) is a material that has a specific melting point, and its latent heat of melting is large enough that it can be used to store thermal energy. This study investigated the effect of size (4–8 Å), and the number of layers (3–10 layers) of iron nanoparticles (NPs) channel on thermal behavior (TB) and phase change (PC) process of sodium sulfate/calcium chloride hexahydrate ($Na_2SO_4/MgCl_2{\cdot}6H_2O$) PCM molecular dynamics (MD) simulation. By increasing the number of layers from 3 to 5, the maximum temperature and heat flux (HF) increased from 406 and 1471 W/m^2 to 451.51 K and 1496 W/m^2. By increasing the number of layers from 3 to 7 layers, the charging time (CT) and discharge time (DT) of atomic samples decreased from 4.01 ns and 4.25 ns to 3.88 ns and 4.17 ns. By adding the iron NPs with a radius of 4, 5, 6, and 8 Å, the maximum temperature increased to 420, 429, 458, and 503 K, respectively. By adding the iron NPs with different radii from 4 to 8 Å, the HF increased from 1566 W/m^2 to 1657 W/m^2. By adding the iron NPs into the $Na_2SO_4/MgCl_2{\cdot}6H_2O$, the received HF increased, and the maximum temperature increased. By adding the iron NPs with different radii, the CT decreased from 3.95 ns to 3.73 ns. The DT increased from 4.33 ns to 4.36 ns by increasing the radius from 4 to 8 Å. According to the TB of this PCM, it should be used in refrigerants instead of toxic and dangerous refrigerants, such as ammonia and chlorofluorocarbon. Moreover, they were used for construction purposes for double-glazed windows.

Abbreviations: PCM, phase change material; NPs, nanoparticles; TB, thermal behavior; PC, phase change; MD, molecular dynamics; HF, heat flux; CT, charging time; DT, discharge time; EAM, embedded-atom method; LJ, Lennard-Jones; LAMMPS, large-scale atomic/molecular massively parallel simulation.

* Corresponding authors at: Nanchang Institute of Technology, 330000, China.
** Corresponding author.
E-mail addresses: m@sztt.org.cn (Y.X. Zhang), shaghaieghbaghaie@yahoo.com (S. Baghaei), wangmengxia@pku.org.cn (M.X. Wang).

https://doi.org/10.1016/j.est.2023.106762
Received 12 September 2022; Received in revised form 17 January 2023; Accepted 22 January 2023
Available online 14 February 2023

Nomenclatures

r_{ij}	the distance between particles (m)
u_i	the potential of a particle (eV)
ε_{ij}	depth of the potential well (kcal/mol)
σ_{ij}	finite distance in which the potential is zero (Å)
r	the distance of the particles from each other
U_{ij}	the electric potential (eV)
V	the total volume of particles ($Å^3$)
k_B	Boltzmann constant (1.380649×10^{-23} $J{\cdot}K^{-1}$)
T	the system temperature (K)
J	the heat flux (W/m^2)
m_i	the mass of the particle (g)
a_i	the acceleration of the particle ($m{\cdot}s^{-2}$)
N_{fs}	the number of degrees of freedom
F_α	constant coefficient between 0 and 1
ρ_β	an attraction force caused by the presence of particles in the simulated box
ϕ_β	a repulsive force caused by atomic charge density

1. Introduction

Most pure materials change the phase among liquid, solid, or gas at certain temperature and pressures [1]. PCM is a material that has a specific melting point, and its latent heat of melting is large enough that it can be used to store thermal energy [2]. PCMs provide a heat capacity from 4 to 15 times that of the conventional storage materials per unit volume, which makes them suitable for use as passive heat control systems. These materials are effectively combined with active heat control to minimize their work cycle and optimize their capacity. Latent thermal storage is one of the most effective methods of accumulating thermal energy [3]. PCMs have found various applications based on their state change temperature. The materials that melt below 15 °C can be used to cool and air condition the room. The materials that melt above 90 °C are used to reduce the temperature in the places where the temperature may suddenly increase and prevent fire [4]. Other PCMs whose melting temperature is between these two values are used for solar energy storage. PCMs have special applications for small-scale cooling and heating (for example, solar refrigerators). PCMs with high melting temperatures can be used in electronic power generation systems. Radiators can be placed next to PCMs to collect solar energy to store energy via the PC at the melting point [5]. Then, this stored energy can be converted into electrical power using the large temperature difference between the radiator and the outside space to operate the thermionic or thermoelectric device. PCMs can be used due to space flight experiments. Many sensitive tests are performed with carefully calibrated instruments [6]. Magnesium dichloride hexahydrate ($MgCl_2{\cdot}6H_2O$) is a magnesium chloride hydrate. This substance is a hydrate, a magnesium halide and an inorganic chloride. The melting temperature of magnesium chloride hexahydrate is higher than 110 °C. Therefore, it can be used as a storage device in solar ovens for indoor cooking or during periods of low solar radiation [7]. This compound is one of the PCM candidates for low temperature applications. This material has advantages, such as relatively high enthalpy, high fusion and heat capacity, as well as high thermal conductivity [7,8]. Sodium sulfate decahydrate crystals are also among hydrated salts with a measurable remaining entropy (entropy at absolute zero) of 6.32 J/K·mol, which proves that this substance is much faster than other water hydrates distributes [9]. The researchers' results show that sodium sulfate and magnesium chloride were used as phase changers in solar cells for construction purposes [10–14].

When the PCMs reach their temperature of PC, the melting point, they absorb a lot of heat without increasing their temperature, and when the temperature of the environment around the PCM decreases by losing the latent heat is stored, they are frozen [15]. The phenomenon of latent heat storage using PCMs brings a higher storage density and a smaller or zero temperature change [16]. In recent years, much experimental research was done on PCMs. For example, Sun et al. [17] investigated the heat transfer of paraffin as a PCM at the temperature range of 26–28 °C. The results show that the melting rate increased as the air temperature, velocity, and inclination angle increased. Han et al. [18] investigated the TB of chloride salts/Al_2O_3, CuO, and ZnO NPs. Their results showed that the type of NPs enhanced thermal conductivity. Using Al_2O_3 NPs, the thermal conductivity increased by 48 %. Kumar et al. [19] studied the effect of Nps on thermal conductivity of PCM. The results show that by adding CuO and Al_2O_3 NPs, the thermal conductivity of PCM increased to 60.56 % and 39.44 %, respectively. Zhang et al. [20] investigated the TB of $CaCl_2{\cdot}6H_2O$-$MgCl_2{\cdot}6H_2O$. The results show that the PCM had excellent thermal conductivity (3.35 W/m·K) and temperature (27.1 °C). Consequently, the introduced material can be used as PCMs. Experimental methods are mostly costly and time-consuming. In recent years, MD simulation methods have attracted the attention of researchers in terms of investigating the complex systems [21–25]. MD simulation is one of the most important tools to study the physical basis of the structure and function of biological macromolecules. Since molecular systems generally include a large number of particles, it is impossible to obtain the properties of complex systems analytically. MD simulation solves this problem using the computational methods. This method created an intermediary between laboratory experiences and theory which was considered a virtual experiment. Ye et al. [26] investigated the TB of NaCl-SiO_2 as PCM with MD simulation. The result show that with SiO_2 (2.4 %) to NaCl, thermal conductivity increased 44.2 %. Zhao et al. [27] studied TB and phonon transport characteristics of CuO/paraffin with MD simulation. Their results show that the thermal properties increased by adding NPs to paraffin. Zhang et al. [28] investigated the effect of NP size on melting point and latent heat of NaCl as PCM. The results show that the structure became more stable by increasing particle size of NaCl atom from 2 nm to 9 nm. In the smaller particle size, the movement of molecules was increased, which destroyed the structure. Yan et al. [29] investigated the thermal properties of erythritol/graphene as PCM with MD simulation. The effects of the graphene mass fraction, size and number of layers on the thermal conductivity and phase transition characteristics, including the melting point and supercooling degree, were analyzed. The simulation results show that the thermal conductivity of composites increased by increasing graphene amount, size and number of layers. Rao et al. [30] investigated the heat and mass transfer mechanisms of the nano-encapsulated and nanoparticle-enhanced PCM by MD simulation. The results show that the appropriate size of particle was very important for heat transfer enhancement of the nanoparticle-enhanced PCM. Hatamle et al. [31] investigated the solar energy capacity of glass in solar collectors with PCM. The results show that maximum density and temperature in fluid particles are 0.09643 atom/$Å^3$ and 1067.51 K. The HF and thermal conductivity reached 650.27 W/m^2 and 0.74 W/m·K, respectively. Li et al. [32] studied the atomic structure of n-octadecane/cooper nanofluids as a PCM using MD simulation method. These simulations show that the regular atomic structure had a thermal diffusivity and a lower melting temperature (phase transition temperature) than the irregular sample. The results show that copper NPs could improve the fluid's thermal properties. Dong et al. [33] studied the thermal properties of macro-capsules PCM with different structures. The results show that oval-shaped capsule had better thermal properties than the sphere capsule. Liu et al. [34] studied the effect of ambient temperatures on the thermal properties of PCMs. The results indicate that by increasing the initial temperature from 30 to 50 °C, the thermal properties of PCM were increased. Liu et al. [35] studied the effects of NPs percentage and the initial temperature on the thermal behavior of the phase transition process of PCM in copper oxide NPs with the MD simulation method. The results show that increasing the initial

Table 1
Parameters of LJ potential function for particles in MD simulation [43,44].

Particle type	σ_{ij} (Å)	ε_{ij} (kcal/mol)
Na	2.983	0.03
S	4.035	0.274
O	3.500	0.06
Mg	3.021	0.111
Cl^-	3.947	0.227
Fe	2.912	0.013

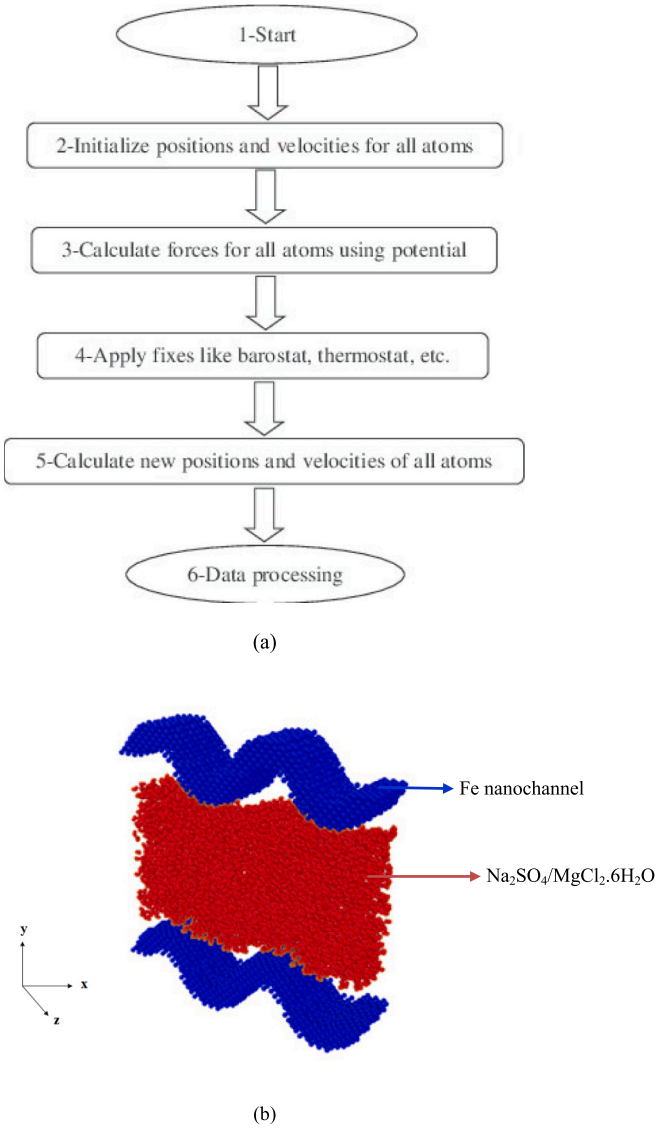

Fig. 1. (a) A general flowchart of the MD simulation [47], (b) atomic arrangement of the simulation, including $Na_2SO_4/MgCl_2{\cdot}6H_2O$ inside the Fe nanochannel.

temperature from 300 to 350 K HF from 1452 to 1770 W/m^2 reduced the phase transition time from 3.92 to 3.73 ns. Xu et al. [36] investigated the TB of aminostaldehyde as the wall and bromohexadecane as a PCM with Au NPs. The results show that thermal conductivity of nanofluid was in range from 1.2 to 1.5 W/m·K. By adding NPs to the base fluid, the thermal properties were improved. Aldossary et al. [37] investigated the TB of decane/silica. The results show that the HF of PCM with NP at 300 K was 1506.3 W/m^2. Svobodova et al. [38] investigated the effect of NPs in molten salts as PCM. The results show that the thermal properties were improved by increasing the particle size.

According to the review of the articles, the size of the particles and the number of channel layers have an effect on the properties of PCM. So far, the effect of these two parameters on $Na_2SO_4/MgCl_2{\cdot}6H_2O$ properties as PCM was not investigated by MD simulation. As a result, this study investigates the effect of particle size (4–8 Å) and the number of layers (3–10 layers) of an iron NPs channel on TB and the PC process of $Na_2SO_4/MgCl_2{\cdot}6H_2O$ as PCM by MD simulation. For this purpose, the CT, DT, HF, and maximum temperature were studied.

2. MD simulation

2.1. MD simulation details

MD simulations produce the information at the microscopic level (position and level of atoms). The conversion of these data into macroscopic values (pressure, energy, etc.) was done by helping the statistical mechanics [53–55]. In MD simulation, Newton's second law was used. The force acting on a particle i can be obtained via the potential function in the form of Eq. (1) [21]:

$$F_i = m_i a_i = -\nabla_i U = -\frac{dU}{dr_i} \tag{1}$$

In Eq. (1), F_i, a_i, m_i, and U represent the force, acceleration, mass of particle i, and a PE function. The secondary location and V of the particles are procured by integrating the equation of Newtonian motion. One of the foremost broadly used of these algorithms is the velocity-Verlet algorithm (Eqs. 2–4) [39,40]:

$$r(t+\Delta t) = r(t) + \Delta t v(t) + \frac{\Delta t^2 a(t)}{2} \tag{2}$$

$$v(t+\Delta t) = v(t) + \Delta t v(t) + \frac{\Delta t\,(a(t) + a(t+\Delta t))}{2} \tag{3}$$

Two different potential functions are required to model the materials under study. EAM potential function [22] describes the interaction among metal particles, a polynomial potential in the first type, which is represented by Eq. (4) [41,42]:

$$U_i = F_\alpha\left(\sum_{i\neq j}\rho_\beta(r_{ij})\right) + \frac{1}{2}\sum_{i\neq j}\phi_\beta(r_{ij}) \tag{4}$$

In Eq. (4), F_α is a constant coefficient between 0 and 1. ρ_β is the attraction force and ϕ_β is the repulsive force. Lennard-Jones (LJ) potential function expresses the interface between metal and non-metallic matrix particles [43].

$$U_{LJ} = 4\varepsilon_{ij}\left[\left(\frac{\sigma_{ij}}{r}\right)^{12} - \left(\frac{\sigma_{ij}}{r}\right)^{6}\right] \tag{5}$$

In Eq. 5, The σ_{ij} is a path where the potential is zero, and ε_{ij} represents the strength of the potential field. The values σ_{ij} and ε_{ij} each of the particles are given in Table 1.

Using the data in Table 1 and Eqs. 6 and 7, the values of σ_{ij} and ε_{ij} for every interactions among the particles are obtained [44]:

$$\varepsilon_{ij} = \sqrt{\varepsilon_i \varepsilon_j} \tag{6}$$

$$\sigma_{ij} = \frac{\sigma_i + \sigma_j}{2} \tag{7}$$

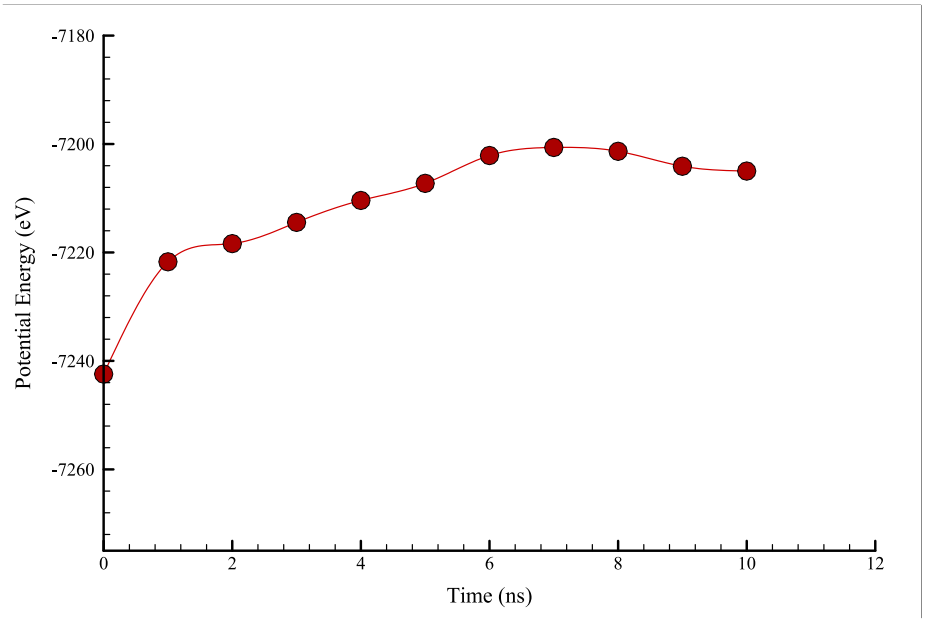

Fig. 2. Changes of potential energy in the simulated sample after 10 ns.

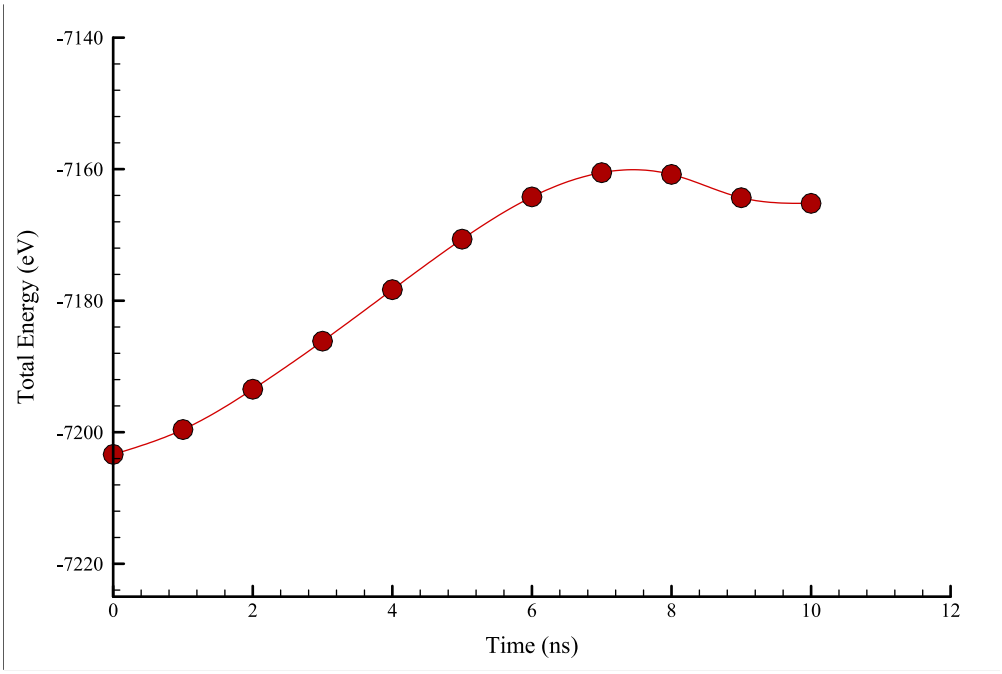

Fig. 3. Changes of total energy in the simulated sample after 10 ns.

HF is obtained from the following equation:

$$J = \frac{1}{V}\left[\sum_i e_i v_i - \sum_i S_i v_i\right]$$
$$= \frac{1}{V}\left[\sum_i e_i v_i - \sum_{i<j} (f_{ij} v_j) x_{ij}\right] \quad (8)$$
$$= \frac{1}{V}\left[\sum_i e_i v_i - \frac{1}{2}\sum_{i<j} (f_{ij} \cdot (v_i + v_j)) x_{ij}\right]$$

In above equation, e_i is the total energy for each particle of the system (kinetic energy + particle potential). v_i, S_i, f_{ij}, and V represent the velocity of the particles, the entropy of the system, the force exerted on the particles i, j, and the total volume of the sample, respectively. The amount of HF flowing in the simulated system was calculated by this sigma.

2.2. Simulation details

The TB and PC processes of $Na_2SO_4/MgCl_2{\cdot}6H_2O$ were studied, in which spherical iron NPs were added to this structure. At first, the structure was modeled with Avogadro software. The main reason for adding NPs to the PCMs was these samples' low charge rate and discharge processes. A nanochannel with Fe type was modeled with a $100 \times 100 \times 200$ nm^3. In this atomic arrangement, periodic boundary

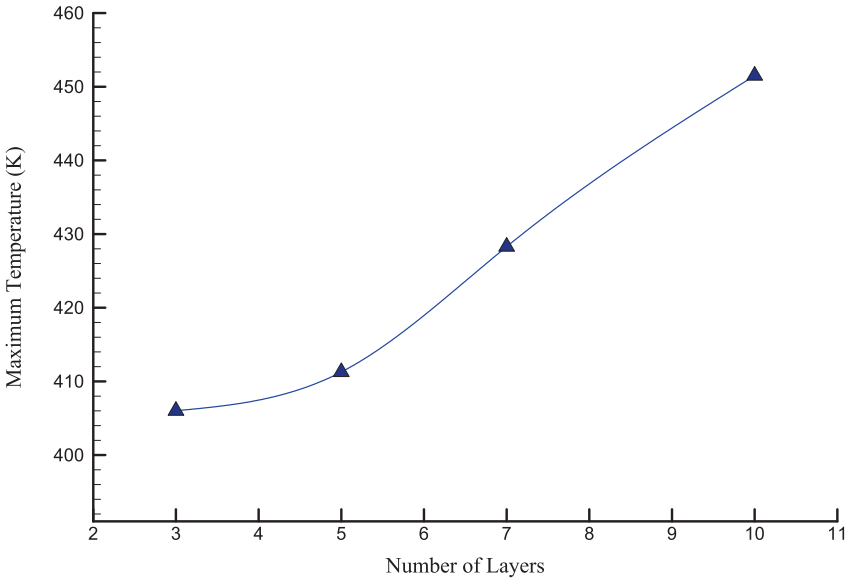

Fig. 4. The maximum temperature changes versus number of layers.

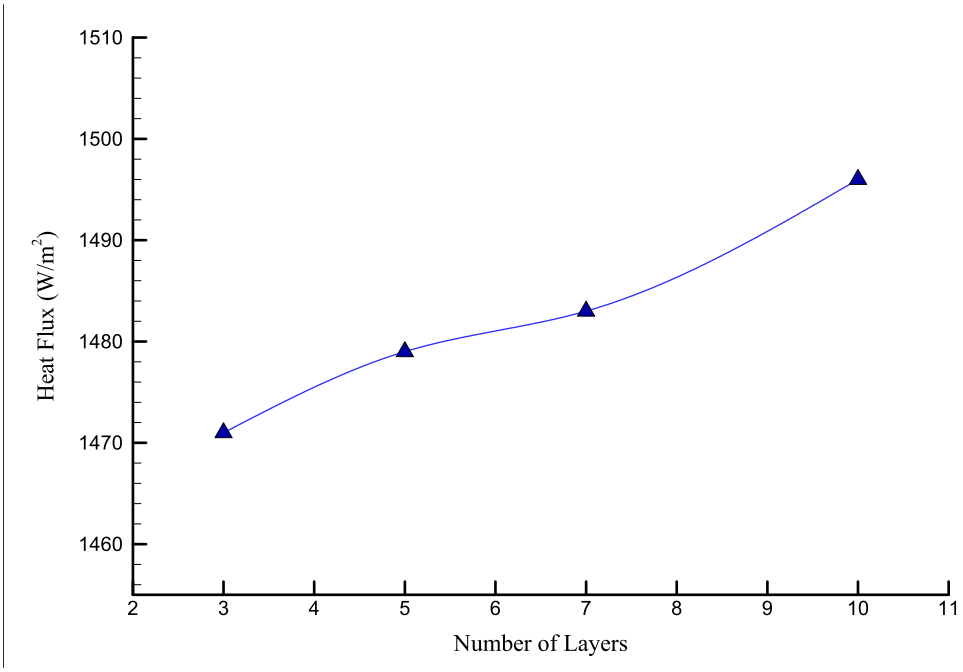

Fig. 5. The HF changes according to the number of layers.

conditions were set along with the y and x axes, and the constant was set to the z-axis. In this step, the NVT ensemble and the Nose-Hoover thermostat set the temperature constant (T = 300 K) by 0.1 ratios for the damping parameter. Avogadro software is one of the best options for drawing chemical structures and checking and analyzing them. Avogadro is an advanced molecular graphics and editor software designed for use in atomic computing, molecular modeling, bioinformatics, materials science, and related fields. Definition of potential functions and related force fields is done in LAMPPS software [45,46]. This initial condition is the set process for t = 10 ns by Δt = 1 fs. A general flowchart of the MD simulation is shown in Fig. 1(a).

The stability of structures was checked by the changes in potential and total energy after 10 ns. Fig. 1(b) shows the atomic arrangement of the simulation, including $Na_2SO_4/MgCl_2{\cdot}6H_2O$ inside the Fe nanochannel.

In the first step of the research, the equilibrium was studied in the simulated samples. Fig. 2 shows the potential energy changes of atomic sample after 10 ns. Based on the results, after 10 ns, the numerical value of this physical property converged to −7204.9 eV. The presence of interaction in the structure, hence its stability, was shown by this convergence in potential energy. More exact, because of the interaction among the particles, the atomic structure possessed the thermodynamic stability in term of the negative energy of the potential. Consequently, the simulated PCM in this research at T = 300 K and P = 1 bar (standard conditions) had thermodynamic equilibrium and physical stability.

Total energy changes were examined to study the overall behavior of

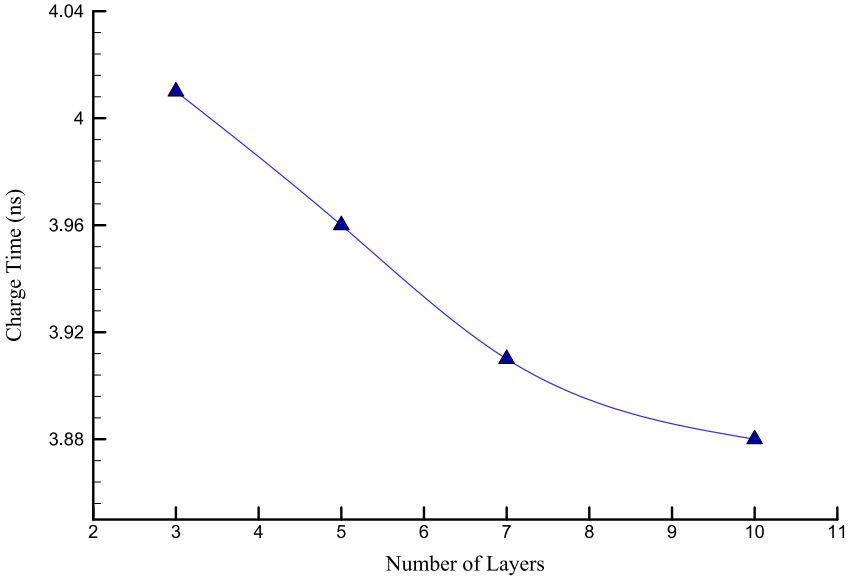

Fig. 6. The CT changes according to the number of layers.

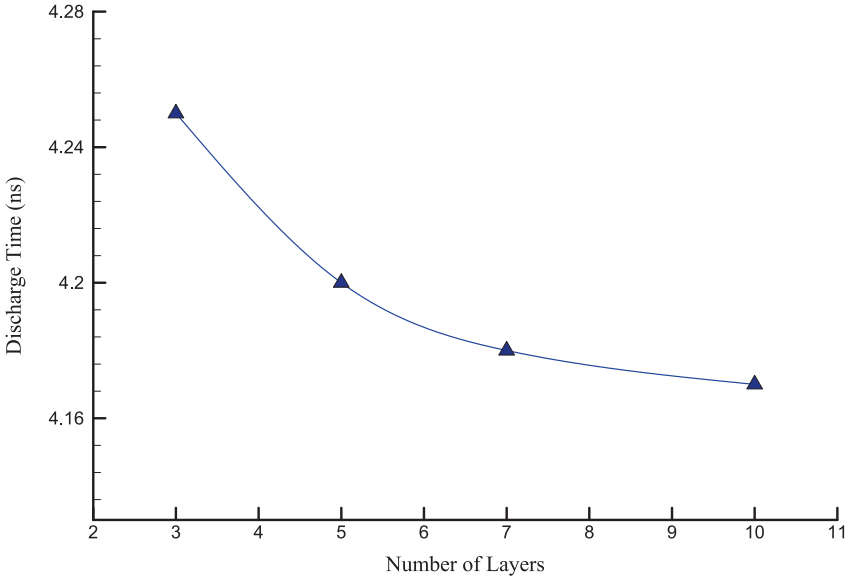

Fig. 7. The changes in the DT according to the number of layers.

simulated structures. In general, the total energy is the sum of kinetic energy and potential energy of simulated structures. The changes in total energy over time (equilibration process time) is shown in Fig. 3. The results show that the total energy value after 10 ns converged to −7165.20 eV. This term's negativity was because of an attraction force among the particles with thermodynamic stability. Therefore, the results show that the simulated structure was structurally stable. Moreover, from the convergence of potential and total energy, it can be concluded that the selected potentials were suitable for simulation. In MD simulation, convergence had a commonly accepted meaning: we found a set of atomic coordinates corresponding to a local energy minimum as a function of chosen force field [48]. The idea of convergence in MD simulation was based on "Ergodic Hypothesis: The long time average was equal to the ensemble average in the limit of an infinite number of members in the ensemble" [49]. As indicated above, it depended on what quantity we were looking at. Convergence of energy (potential, kinetic, total), temperature, etc. The convergence of total energy and potential energy was studied. Considering the convergence of total energy to −7165.20 eV and potential energy to −7204.9 eV, the simulated structures were stable. Furthermore, the selected potential function was suitable for simulation.

3. Results

3.1. The effects of the number of layers

This section studied the simulation of atomic channels with the number of layers 3, 5, 7, and 10 layers. Fig. 4 shows the maximum temperature changes based on the number of atomic channel layers. The results show that by increasing the number of atomic layers, the HF

Table 2
The maximum temperature, charge, and DT change according to the number of layers.

Number of layers	Maximum temperature (K)	HF (W/m^2)	CT (ns)	DT (ns)
3	406.02	1471	4.01	4.25
5	411.28	1479	3.96	4.20
7	428.29	1483	3.91	4.18
10	451.51	1496	3.88	4.17

Table 3
The results of Yan et al. [29] research.

Number of layers	Maximum temperature (K)
1	379.13
2	385.37
3	387.37
4	391.60

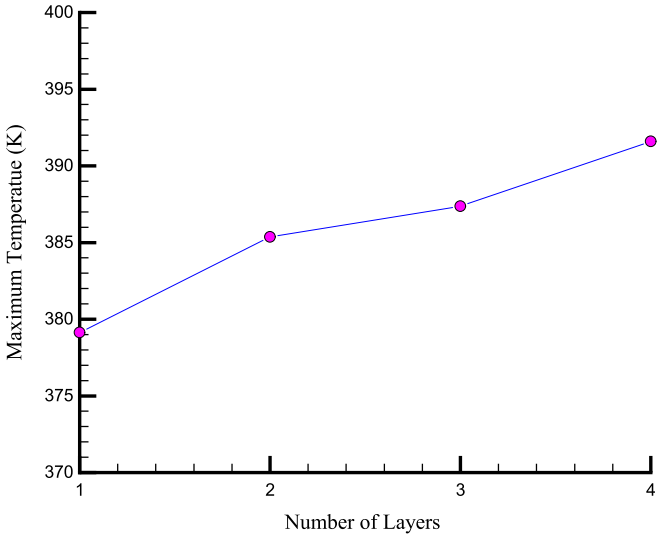

Fig. 8. The results of Yan et al. [29] research.

increased, and as a result, the maximum temperature in the simulated sample increased. By increasing the number of layers from 3 to 10, the maximum temperature increased from 406 to 451.51 K. By increasing the maximum temperature, atomic movement increased, and atoms freely moved. This increase in maximum temperature caused the number of atomic collisions in the simulated sample to increase over time. With the increase in maximum temperature, atomic movement increases, and atoms moved freely. This increase in maximum temperature causes the number of atomic collisions in the simulated sample to increase over time. From an atomic point of view, increasing initial temperature led to increased atomic motion, thus reducing the charging and discharging time. More precisely $\frac{1}{2}mv^2 = \frac{3}{2}kT$, kinetic energy (movement of atoms) and the initial temperature of atomic sample were directly related to each other.

Fig. 5 shows the HF changes based on the number of layers. Temperature and pressure in the structures were set to 300 K and 1 bar to study the HF changes. According to Fig. 5, by increasing the number of layers in the atomic channel from 3 to 10, the HF increased from 1471 to 1496 W/m^2. The increase in maximum temperature caused the number of atomic collisions in the simulated sample to increase. Consequently, the HF was transferred more intensively, improving the structure's TB. By increasing the number of layers, the number of iron atoms per unit of heat transfer surface increases. More atoms are related to PCM. On the other hand, with the increase in the number of layers, the movement of molecules and their vibrations increase [29]. As a result, with increasing temperature, the kinetic energy of atoms increases and as a result HF increases.

Charging and discharging processes follow an isothermal behavior. PCMs continue to absorb heat without significantly increasing temperature until all materials are in the liquid phase. When the temperature around the liquid decreases, the PCM freezes and dissemination its latent cumulative heat [35]. Fig. 6 shows the CT changed based on the number of layers. According to Fig. 6, by increasing the number of layers from 3 to 10 layers, the CT of atomic samples decreased from 4.01 ns to 3.88 ns. As the maximum temperature increased, the HF increased and quickly changed from one state to another and changes phase. As a result, the CT of the sample decreased. As the maximum temperature increases, the HF increases and quickly changes from one state to another and changes phase. As a result, the CT of the sample decreases.

Fig. 7 shows the changes in the DT based on the number of layers. By increasing the number of layers from 3 to 10, the DT of atomic samples decreased from 4.25 ns to 4.17 ns. Reducing the charging and DT of the studied sample was a positive phenomenon in terms of thermal applications to perform processes, such as heat transfer and cooling of nanostructures. Reducing the charging and DT of the studied sample is a positive phenomenon in terms of thermal applications to perform processes such as heat transfer and cooling of nanostructures.

Table 2 shows the value of HF, charge, and DT of atomic samples according to the number of layers. According to Table 2, by increasing the number of layers, the maximum temperature and HF increased in terms of the increase in atomic oscillations and collisions. By increasing the HF, the charge and DT decreased from 4.01 ns to 3.88 ns and 4.25 ns to 4.17 ns, respectively, by increasing the number of layers from 3 to 10.

Yan et al. [29] investigated the thermal properties of erythritol/graphene as PCM with MD simulation. The effects of graphene mass fraction, size and number of layers on the thermal conductivity and phase transition characteristics, including the melting point and supercooling degree, were analyzed. Table 3 and Fig. 8 show the results of Yan et al. [29] research. The simulation results show that the thermal conductivity of composites increased by increasing graphene amount, size and number of layers. The results are consistent with the results of this paper.

3.2. The effects of the iron NPs size

Iron NPs with different dimensions (between 10 nm and 100 nm) are used in the industry. Research has shown that different sizes of NPs have different properties [50,51]. As a result, in this research, the dimensions of iron NPs were investigated. Adding iron NPs to PCM can significantly improve TB. In this section, we added spherical NPs of iron with a radius of 4, 5, 6, and 8 Å into the $Na_2SO_4/MgCl_2{\cdot}6H_2O$ structure and investigated its PC process and TB. Fig. 9 shows the atomic arrangement of simulated samples based on the radius of iron NPs. Based on Fig. 9, by increasing the radius up to 8 Å, the aggregation process in the structure was not observed after 10 ns. As a result, the defined sample had thermodynamic equilibrium and physical stability.

Fig. 10 shows the maximum temperature changes of $Na_2SO_4/MgCl_2{\cdot}6H_2O$-iron NPs structure after 10 ns. By adding iron NPs with a radius of 4, 5, 6, and 8 Å, the maximum temperature increased to 420, 429, 458, and 503 K, respectively. With the increase in maximum temperature, atomic movement increases, and atoms moved freely. This increase in maximum temperature causes the number of atomic collisions in the simulated sample to increase over time.

Fig. 11 shows the HF changes in the sample of $Na_2SO_4/MgCl_2{\cdot}6H_2O$-iron NPs based on the radius. By adding the iron NPs with different radii from 4 to 8 Å, the HF increased from 1566 W/m^2 to 1657 W/m^2. By adding the iron NPs into the $Na_2SO_4/MgCl_2{\cdot}6H_2O$, the received HF increased, and the maximum temperature increased. This increase in maximum temperature corresponded to the larger oscillation

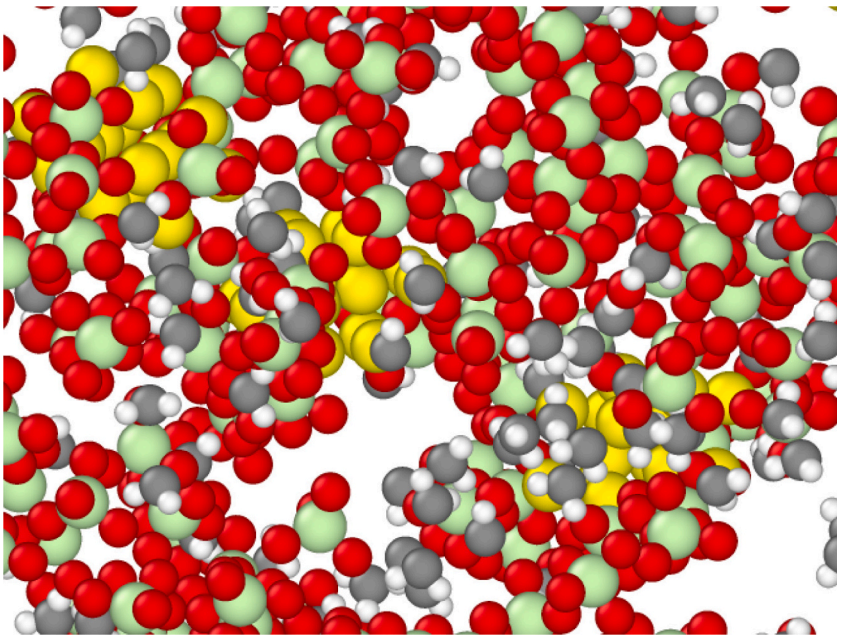

(a)

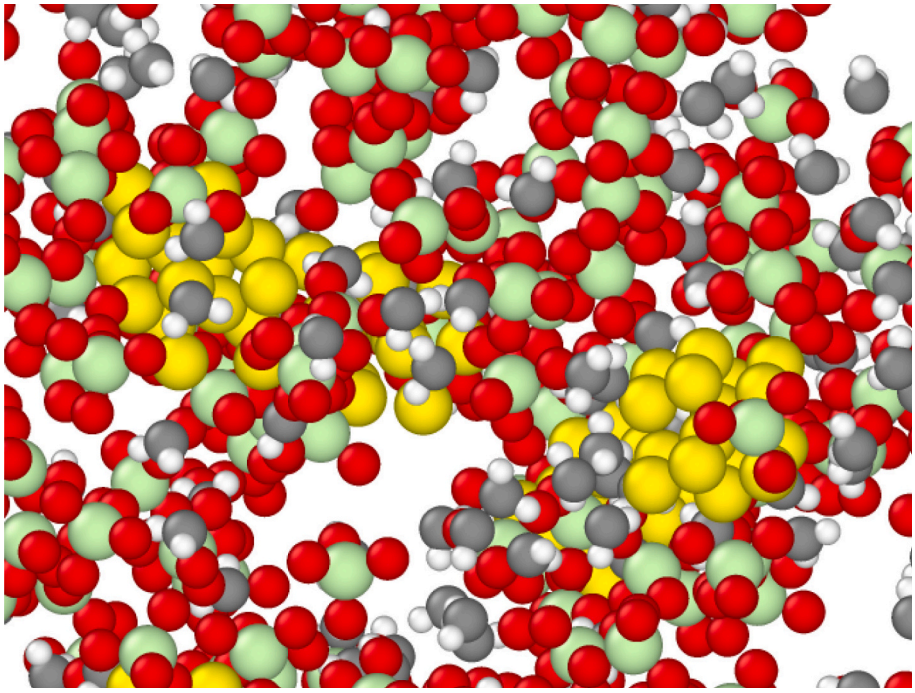

(b)

Fig. 9. Evolution of the $Na_2SO_4/MgCl_2{\cdot}6H_2O$ structure in the presence of iron NPs with radius a) 4 Å, b) 5 Å, c) 6 Å, d) 8 Å after 10 ns.

range of the atoms and, consequently, the increase in the HF inside the simulation box. As the particle radius becomes larger, the available surface area increases. As a result, heat transfer increases as the available surface increases.

Compared to the results of other researchers, Zhang et al.'s results showed that increasing the diameter of NPs from 2 nm to 9 nm increased thermal properties [28]. Fig. 12 and Table 4 show the results of Zhang et al. [28] research. According to Fig. 12 by increasing the size of NPs from 2 nm to 9 nm the temperature increasing from 838.35 K to 1000.42 K. The results are consistent with the results of this paper.

Fig. 13 shows the CT changes of the $Na_2SO_4/MgCl_2{\cdot}6H_2O$-iron NPs in terms of the radius. According to Fig. 13, the CT decreased by increasing the radius of iron NPs. From a numerical point of view, by adding the iron NPs with different radii, the CT decreased from 3.95 ns to 3.73 ns.

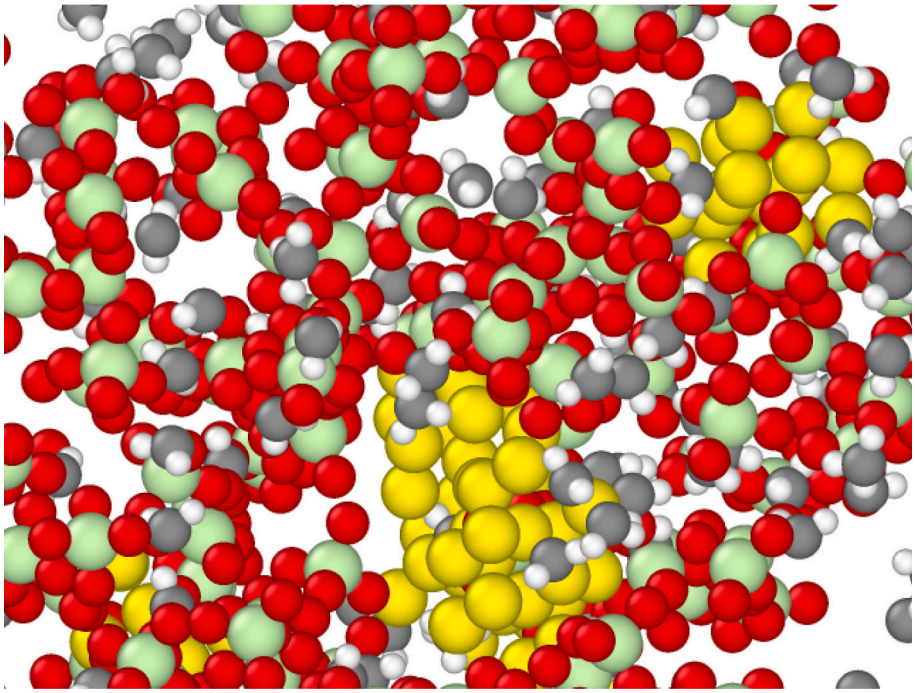

(c)

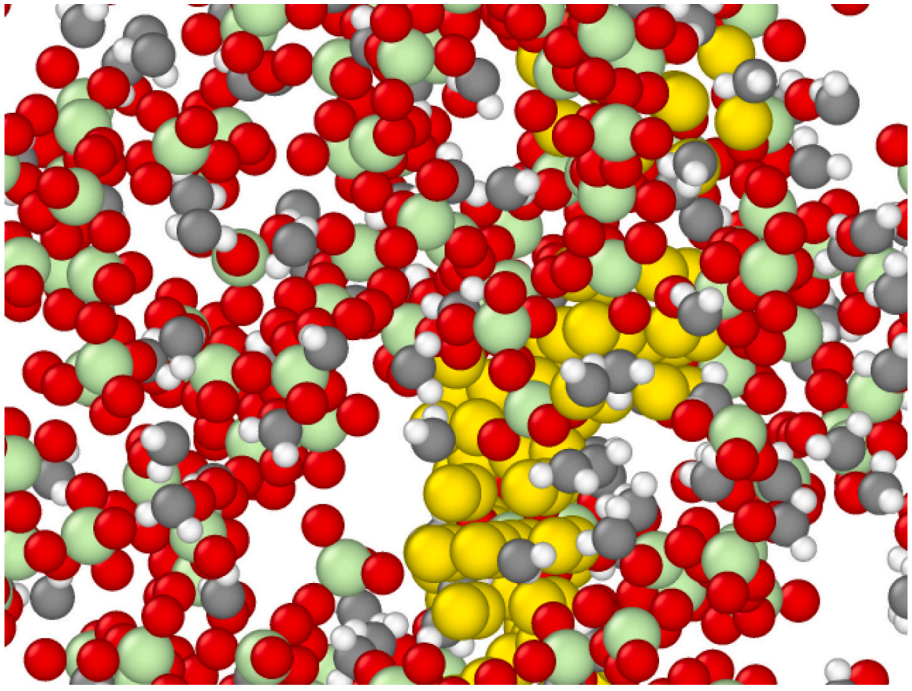

(d)

Fig. 9. (*continued*).

As the maximum temperature increased, the HF increased and quickly changed from one state to another and changes phase. As a result, the CT of the sample decreased.

On the other hand, the presence of iron NPs increased the DT of the sample, which made the $Na_2SO_4/MgCl_2{\cdot}6H_2O$-iron NPs an attractive option for various heat transfer processes. Fig. 14 shows the DT changes of the $Na_2SO_4/MgCl_2{\cdot}6H_2O$-iron NPs according to the radius. The DT increased from 4.33 ns to 4.36 ns by increasing the radius from 4 to 8 Å. As the maximum T increases, the HF increases and quickly changes from one state to another and changes phase. As a result, the CT of the sample decreases. This reduction in charge and DT in the structure of the atomic microcapsules increased its efficiency.

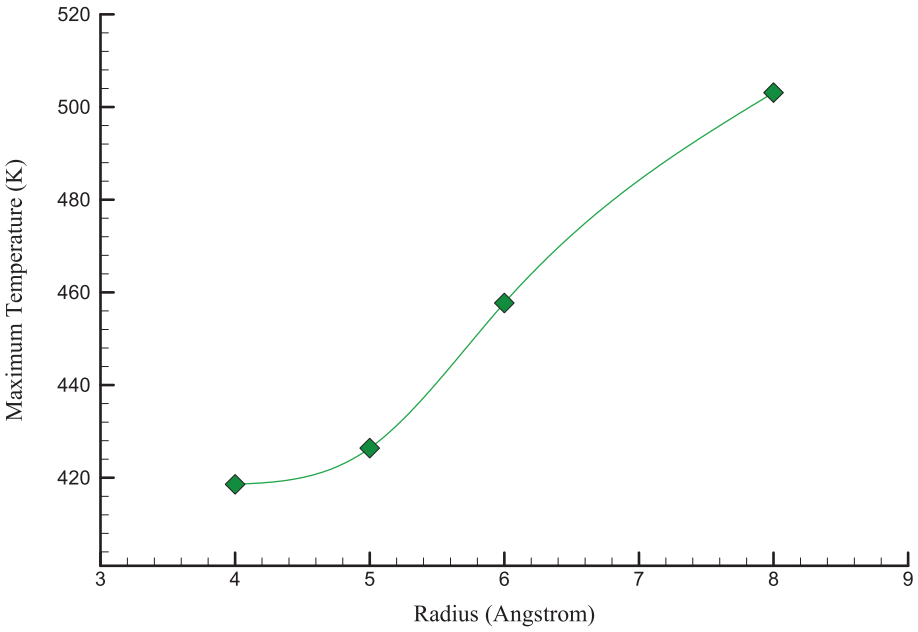

Fig. 10. The maximum temperature changes according to the radius.

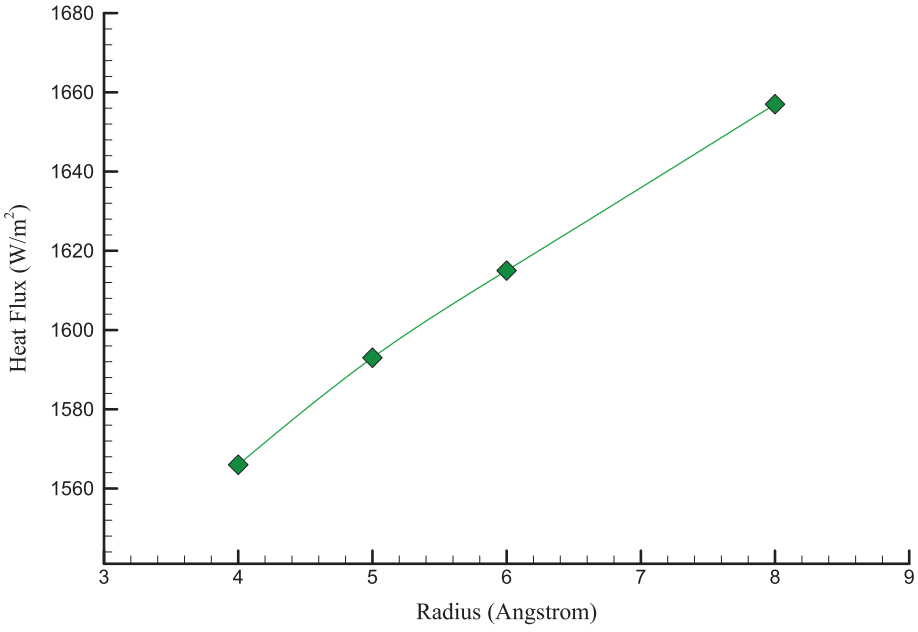

Fig. 11. The HF changes of the $Na_2SO_4/MgCl_2{\cdot}6H_2O$-iron NPs according to the radius.

Table 5 shows the value of HF, charge, and DT of atomic samples based on the radius. According to Table 5, by increasing the radius of NPs, the maximum temperature and HF increases in terms of the increased atomic oscillations and the number of collisions. By increasing, the HF, the CT decreased from 3.95 ns to 3.73, and the DT increases from 4.33 ns to 4.36 ns by increasing the radius from 4 to 8 Å.

4. Conclusion

This study investigated the effect of particle size (4–8 Å) and the number of layers (3–10 layers) of an iron NPs channel on TB and PC process of $Na_2SO_4/MgCl_2{\cdot}6H_2O$) as PCM by MD simulation. For this purpose, the CT, DT, HF, and maximum temperature were studied. The results are as follows:

- The potential and total energy converged to −7204.99 eV and −7165.2 eV, respectively. This convergence indicated the proper selection of the potential function and sufficient time for structural equilibrium.
- By increasing the number of layers from 3 to 10, the maximum temperature increased from 406 to 451.51 K.
- By increasing the number of layers in the atomic channel from 3 to 10, the HF increased from 1471 to 1496 W/m^2. The increase in temperature caused the number of atomic collisions in the simulated sample to increase.
- By increasing the number of layers from 3 to 10 layers, the CT of atomic samples decreased from 4.01 ns to 3.88 ns. As the temperature increased, the HF quickly increased, the changes from one state

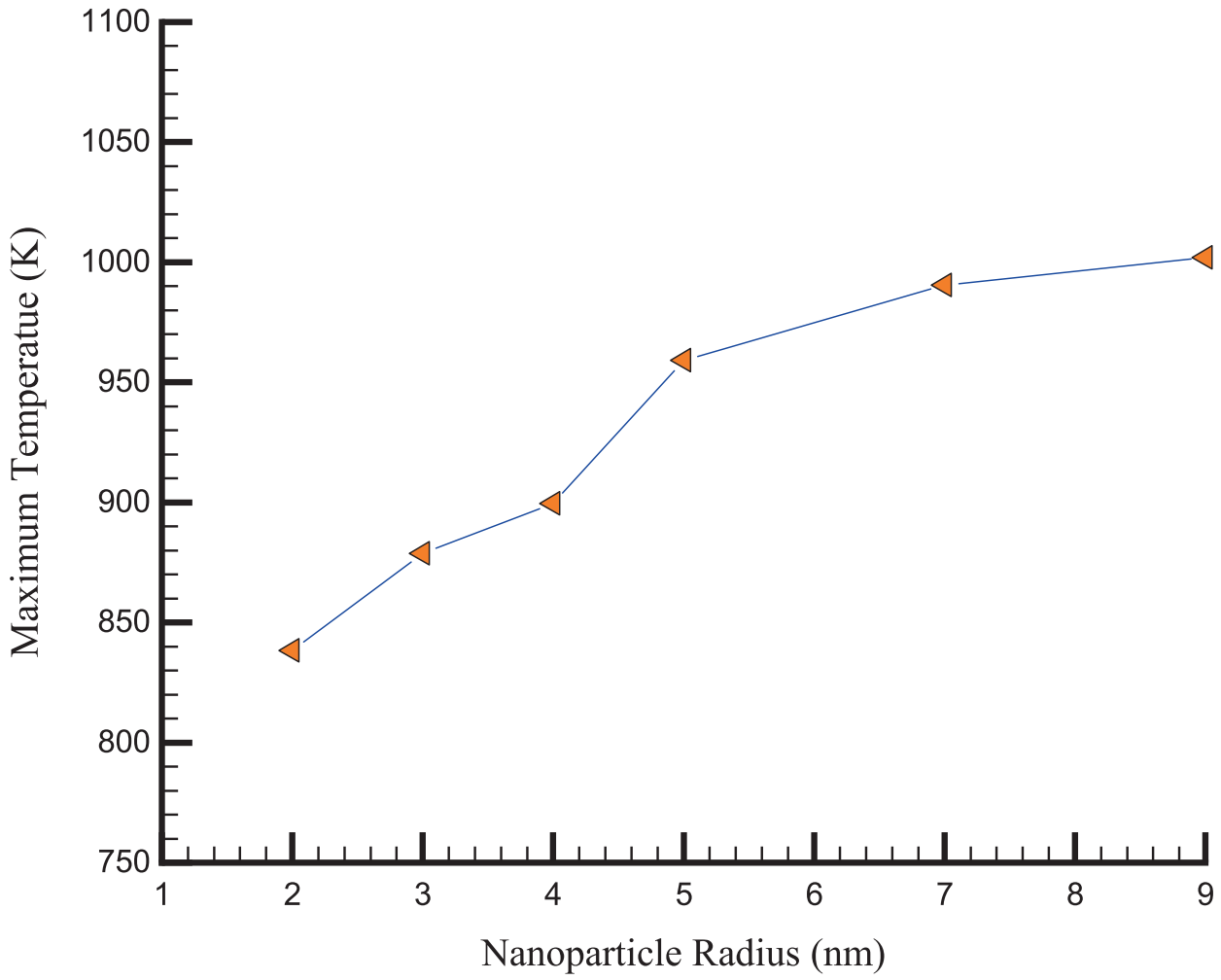

Fig. 12. The results of Zhang et al. [28] research.

Table 4
The results of Zhang et al. [28] research.

NP size	Maximum temperature (K)
2	838.38
3	887.82
4	899.46
5	959.08
7	990.42
9	1000.42

to another, and changes phase. Consequently, the CT of the sample decreased.

- By increasing the number of layers from 3 to 10, the DT of atomic samples decreased from 4.25 ns to 4.17 ns. Reducing the charging and DT of the studied sample was a positive phenomenon in terms of thermal applications to perform processes, such as heat transfer and cooling of nanostructures.
- By adding iron NPs with a radius of 4, 5, 6, and 8 Å, the maximum temperature increases to 420, 429, 458, and 503 K, respectively.
- By adding the iron NPs with different radii from 4 to 8 Å, the HF increases from 1566 W/m^2 to 1657 W/m^2. By adding the iron NPs into the $Na_2SO_4/MgCl_2{\cdot}6H_2O$, the received HF increases, and the maximum temperature increases.
- By adding the iron NPs with different radii, the CT decreases from 3.95 ns to 3.73 ns.
- The DT increases from 4.33 ns to 4.36 ns by increasing the radius from 4 to 8 Å.

According to the thermal properties of this PCM, it should be used in refrigerants instead of toxic and dangerous refrigerants, such as ammonia and chlorofluorocarbon. Moreover, they were used for construction purposes for double-glazed windows.

To improve the performance of PCM, the authors suggest to add graphene particles and carbon tubes to them, and also to study the application of variable HF on the wall and the effects of temperature on the thermal properties of this PCM.

CRediT authorship contribution statement

- The corresponding author is responsible for ensuring that the descriptions are accurate and agreed by all authors.
- The role(s) of all authors are listed.
- Authors have contributed in multiple roles.

Declaration of competing interest

The authors declare that they have no known competing financial interests or personal relationships that could have appeared to influence the work reported in this paper.

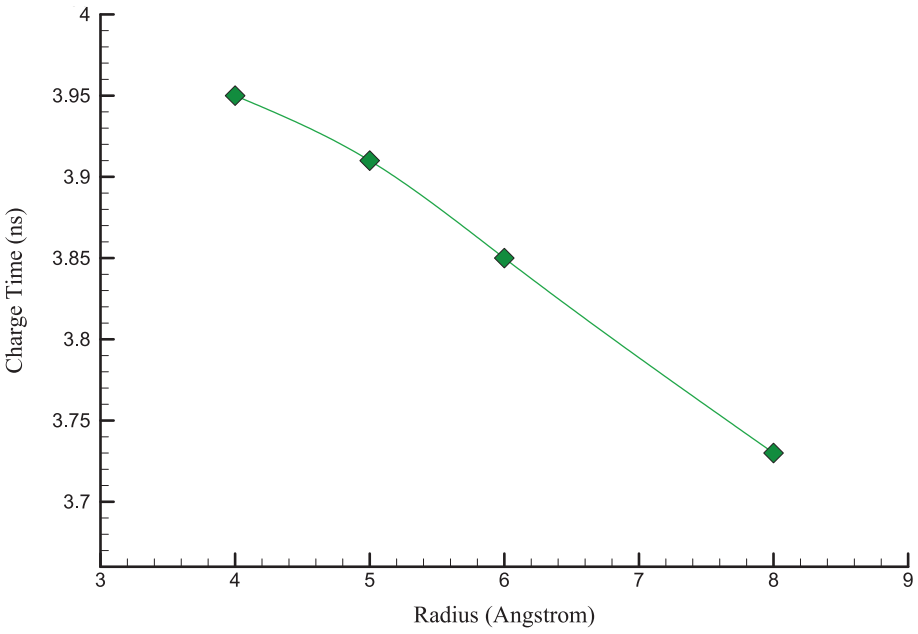

Fig. 13. The CT changes of the $Na_2SO_4/MgCl_2{\cdot}6H_2O$-iron NPs in terms of the radius.

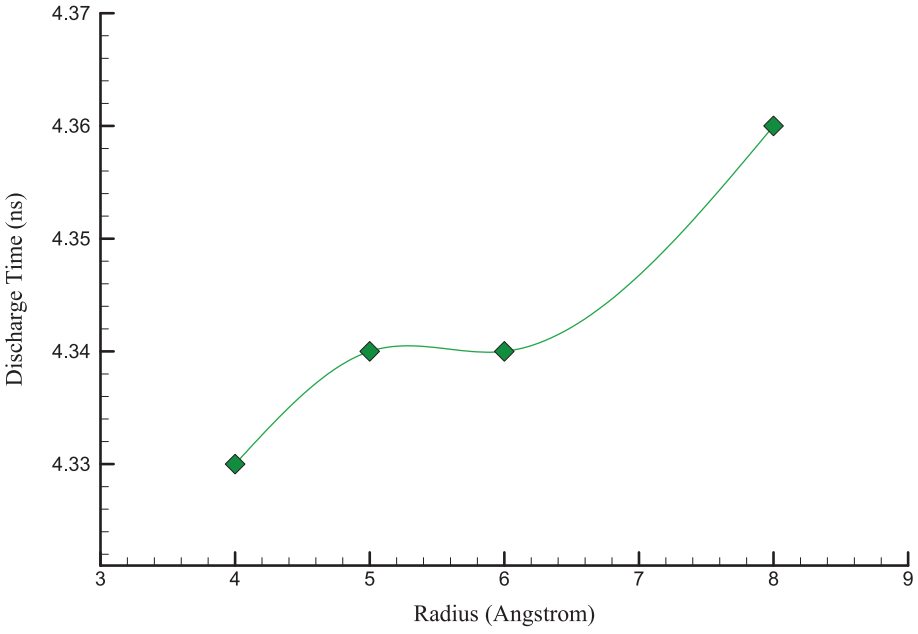

Fig. 14. The DT changes of the $Na_2SO_4/MgCl_2{\cdot}6H_2O$-iron NPs according to the radius.

Table 5
The maximum temperature, charge, and DT change according to the radius.

Radius (Å)	Maximum temperature (K)	HF (W/m^2)	CT (ns)	DT (ns)
4	418.58	1566	3.95	4.33
5	426.39	1593	3.91	4.34
6	457.71	1615	3.85	4.34
8	503.11	1657	3.73	4.36

Data availability

No data was used for the research described in the article.

Acknowledgements

This research is supported by CDAS-2022-07, a major project of the China Doctoral Association's Science and Technology Innovation Promotion Program for Overseas High-level Talents.

References

[1] K.A. Ismail, F.A. Lino, P.L.O. Machado, M. Teggar, M. Arıcı, T.A. Alves, M.P. Teles, New potential applications of phase change materials: a review, J. Energy Storage 53 (2022), 105202.

[2] S. Sikiru, T.L. Oladosu, T.I. Amosa, S.Y. Kolawole, H. Soleimani, Recent advances and impact of phase change materials on solar energy: a comprehensive review, J. Energy Storage 53 (2022), 105200.
[3] L.G. Socaciu, Thermal energy storage with phase change material, Leonardo Electron. J. Pract. Technol. 20 (2012) 75–98.
[4] A. Sharma, V.V. Tyagi, C.R. Chen, D. Buddhi, Review on thermal energy storage with phase change materials and applications, Renew. Sust. Energ. Rev. 13 (2) (2009) 318–345.
[5] J. Jaguemont, N. Omar, P. Van den Bossche, J. Mierlo, Phase-change materials (PCM) for automotive applications: a review, Appl. Therm. Eng. 132 (2018) 308–320.
[6] K. Faraj, M. Khaled, J. Faraj, F. Hachem, C. Castelain, Phase change material thermal energy storage systems for cooling applications in buildings: a review, Renew. Sust. Energ. Rev. 119 (2020), 109579.
[7] A. El-Sebaii, S. Al-Heniti, F. Al-Agel, A. Al-Ghamdi, F. Al-Marzouki, One thousand thermal cycles of magnesium chloride hexahydrate as a promising PCM for indoor solar cooking, Energy Convers. Manag. 52 (4) (2011) 1771–1777.
[8] R. Pilar, L. Svoboda, P. Honcova, L. Oravova, Study of magnesium chloride hexahydrate as heat storage material, Thermochim. Acta 546 (2012) 81–86.
[9] D.E. Garrett, Sodium Sulfate: Handbook of Deposits, Processing, Properties, and Use, Academic press, 2001.
[10] C. Zhang, Z. Zhang, R. Ye, X. Gao, Z. Ling, Characterization of MgCl2· 6H2O-based eutectic/expanded perlite composite phase change material with low thermal conductivity, Materials 11 (12) (2018) 2369.
[11] S. Höhlein, A. König-Haagen, D. Brüggemann, Thermophysical characterization of MgCl2· 6H2O, xylitol and erythritol as phase change materials (PCM) for latent heat thermal energy storage (LHTES), Materials 10 (4) (2017) 444.
[12] V. Saikrishnan, A. Karthikeyan, N. Beemkumar, S. Ganesan, D. Yuvarajan, The thermal performance analyses of the solar energy-powered thermal energy storage system with MgCl2· 6H2O as PCM, J. Braz. Soc. Mech. Sci. Eng. 42 (1) (2020) 1–9.
[13] M.N. Islam, D.H. Ahmed, Delaying the temperature fluctuations through PCM integrated building walls—Room conditions, PCM placement, and temperature of the heat sources, Energy Storage 3 (5) (2021), e245.
[14] L. Meng, A.S. Ivanov, S. Kim, X. Zhao, N. Kumar, A. Young-Gonzales, T. Saito, W. Bras, K. Gluesenkamp, V. Bocharova, Alginate–Sodium sulfate decahydrate phase change composite with extended stability, ACS Appl. Polym. Mater. 4 (9) (2022) 6563–6571.
[15] T. Zhou, Y. Xiao, Y. Liu, J. Lin, H. Huang, Research on cooling performance of phase change material-filled earth-air heat exchanger, Energy Convers. Manag. 177 (2018) 210–223.
[16] B. Zalba, J.M. Marın, L.F. Cabeza, H. Mehling, Review on thermal energy storage with phase change: materials, heat transfer analysis and applications, Appl. Therm. Eng. 23 (3) (2003) 251–283.
[17] X. Sun, Y. Chu, Y. Mo, S. Fan, S. Liao, Experimental investigations on the heat transfer of melting phase change material (PCM), Energy Procedia 152 (2018) 186–191.
[18] D. Han, B.G. Lougou, Y. Xu, Y. Shuai, X. Huang, Thermal properties characterization of chloride salts/nanoparticles composite phase change material for high-temperature thermal energy storage, Appl. Energy 264 (2020), 114674.
[19] P.M. Kumar, D. Sudarvizhi, P.M.J. Stalin, A. Aarif, R. Abhinandhana, A. Renuprasanth, V. Sathya, N.T. Ezhilan, Thermal characteristics analysis of a phase change material under the influence of nanoparticles, Mater. Today Proc. 45 (2021) 7876–7880.
[20] Y. Zhang, X. Zhang, Thermal properties of a new type of calcium chloride hexahydrate-magnesium chloride hexahydrate/expanded graphite composite phase change material and its application in photovoltaic heat dissipation, Sol. Energy 204 (2020) 683–695.
[21] G. Kurt, N. Yaşar, Comparison of experimental, analytical and simulation results for hot rolling of S275JR quality steel, J. Mater. Res. Technol. 9 (3) (2020) 5204–5215.
[22] P. Alipour, et al., Modeling different structures in perturbed Poiseuille flow in a nanochannel by using of molecular dynamics simulation: Study the equilibrium, Phys. A 515 (2019) 13–30.
[23] X. Liu et al., A molecular dynamics study of thermal behavior of ammonia/Cu nanorefrigerant flow under different initial pressures and electric fields, J. Mol. Liquids. 367 (2022), 120388.
[24] P. Alipour, et al., Molecular dynamics simulation of fluid flow passing through a nanochannel: effects of geometric shape of roughnesses, J. Mol. Liquids 275 (2019) 192–203.
[25] H. Zeng, et al., Investigation of mechanical and thermal characteristics of epoxy/graphene oxide nanocomposites by molecular dynamics simulation, Mater. Sci. Eng. B. 287 (2023), 116087.
[26] Y. Yu, Y. Tao, Y.-L. He, Molecular dynamics simulation of thermophysical properties of NaCl-SiO2 based molten salt composite phase change materials, Appl. Therm. Eng. 166 (2020), 114628.
[27] C. Zhao, Y. Tao, Y. Yu, Molecular dynamics simulation of thermal and phonon transport characteristics of nanocomposite phase change material, J. Mol. Liq. 329 (2021), 115448.
[28] S. Zhang, Y. Jin, Y. Yan, Depression of melting point and latent heat of molten salts as inorganic phase change material: size effect and mechanism, J. Mol. Liq. 346 (2022), 117058.
[29] X. Yan, H. Zhao, Y. Feng, L. Qiu, L. Lin, X. Zhang, T. Ohara, Excellent heat transfer and phase transformation performance of erythritol/graphene composite phase change materials, Compos. Part B 228 (2022), 109435.
[30] Z. Rao, S. Wang, F. Peng, Molecular dynamics simulations of nano-encapsulated and nanoparticle-enhanced thermal energy storage phase change materials, Int. J. Heat Mass Transf. 66 (2013) 575–584.
[31] R.I. Hatamleh, N.H. Abu-Hamdeh, A. Khoshaim, M.A. Alzahrani, Using phase change material (PCM) to improve the solar energy capacity of glass in solar collectors by enhancing their thermal performance via developed MD approach, Eng. Anal. Boundary Elements 143 (2022) 163–169.
[32] Q. Li, Y. Yu, Y. Liu, C. Liu, L. Lin, Thermal properties of the mixed n-octadecane/Cu nanoparticle nanofluids during phase transition: a molecular dynamics study, Materials 10 (1) (2017) 38.
[33] Y. Dong, F. Wang, Y. Zhang, X. Shi, A. Zhang, Y. Shuai, Experimental and numerical study on flow characteristic and thermal performance of macro-capsules phase change material with biomimetic oval structure, Energy 238 (2022), 121830.
[34] J. Liu, Y. Fan, Q. Xie, An experimental study on the thermal performance of mixed phase change materials-based battery cooling system, J. Energy Storage 46 (2022), 103839.
[35] X. Liu, M. Adibi, M. Shahgholi, I. Tlili, S.M. Sajadi, A. Abdollahi, Z. Li, A. Karimipour, Phase change process in a porous carbon-paraffin matrix with different volume fractions of copper oxide nanoparticles: a molecular dynamics study, J. Mol. Liq. 366 (2022), 120296.
[36] L. Xu, Y. Zhang, J. Li, L. Zhang, Z. Yuan, H.S. Majdi, M. Hekmatifar, Thermal behavior and phase transition of the aminostaldehyde as the wall and bromohexadecane as a phase change material enriched via gold nanoparticles: molecular dynamics study, J. Energy Storage 55 (2022), 105482.
[37] A.S. Aldossary, N. Sulaiman, PCM examine of silica/decane nanostructure in the presence of copper oxide nanoparticles to improve the solar energy capacity of glass in the solar collectors via MD approach, Eng. Anal. Boundary Elements 145 (2022) 72–82.
[38] A. Svobodova-Sedlackova, C. Barreneche, G. Alonso, A.I. Fernandez, P. Gamallo, Effect of nanoparticles in molten salts–MD simulations and experimental study, Renew. Energy 152 (2020) 208–216.
[39] W.C. Swope, H.C. Andersen, P.H. Berens, K.R. Wilson, A computer simulation method for the calculation of equilibrium constants for the formation of physical clusters of molecules: application to small water clusters, J. Chem. Phys. 76 (1) (1982) 637–649.
[40] E. Hairer, C. Lubich, G. Wanner, Geometric numerical integration illustrated by the Störmer-Verlet method, Acta Numer. 12 (2003) 399–450.
[41] A. Mosavi, M. Hekmatifar, A.A. Alizadeh, D. Toghraie, R. Sabetvand, A. Karimipour, The molecular dynamics simulation of thermal manner of Ar/Cu nanofluid flow: the effects of spherical barriers size, J. Mol. Liq. 319 (2020), 114183.
[42] M.S. Daw, M.I. Baskes, Embedded-atom method: derivation and application to impurities, surfaces, and other defects in metals, Phys. Rev. B 29 (12) (1984) 6443.
[43] A.K. Rappé, C.J. Casewit, K. Colwell, W.A. Goddard III, W.M. Skiff, UFF, a full periodic table force field for molecular mechanics and molecular dynamics simulations, J. Am. Chem. Soc. 114 (25) (1992) 10024–10035.
[44] H. Berendsen, J. Grigera, T. Straatsma, The missing term in effective pair potentials, J. Phys. Chem. 91 (24) (1987) 6269–6271.
[45] S. Nosé, A unified formulation of the constant temperature molecular dynamics methods, J. Chem. Phys. 81 (1) (1984) 511–519.
[46] W.G. Hoover, Canonical dynamics: equilibrium phase-space distributions, Phys. Rev. A 31 (3) (1985) 1695.
[47] M. Foroutan, and S. M. Fatemi, "Molecular Dynamics Simulations of Systems Containing Nanostructures.".
[48] L.J. Smith, X. Daura, W.F. van Gunsteren, Assessing equilibration and convergence in biomolecular simulations, Proteins: Struct., Funct., Bioinf. 48 (3) (2002) 487–496.
[49] A. Henriksson, On the Ergodic Theorem and Information Loss in Statistical Mechanics, 2019.
[50] A. Arjmandfard, D. Toghraie, B. Mehmandoust, M. Hashemian, A. Karimipour, Study the time evolution of nanofluid flow in a microchannel with various sizes of Fe nanoparticle using molecular dynamics simulation, Int. Commun. Heat Mass Transfer 118 (2020), 104874.
[51] Y.A. Koksharov, Magnetism of nanoparticles: effects of size, shape, and interactions, Magn. Nanoparticles (2009) 197–254.
[53] D.T. Semiromi, A.R. Azimian, Molecular dynamics simulation of nonodroplets with the modified Lennard-Jones potential function, Heat Mass Transf. 47 (2011) 579–588, https://doi.org/10.1007/s00231-010-0747-7.
[54] D.T. Semiromi, A.R. Azimian, Molecular dynamics simulation of annular flow boiling with the modified Lennard-Jones potential function, Heat Mass Transfer 48 (2012) 141–152, https://doi.org/10.1007/s00231-011-0855-z.
[55] X. Liu, I. Patra, O.R. Kuzichkin, M. Zaidi, S.M. Abdulnabi, Z. Mohsen Najm, U. S. Altimari, S.K. Hadrawi, M. Taheri Andani, M. Hekmatifar, Molecular dynamics study of the effect of external electric field amplitude and cavity on thermal properties of Ammonia/Copper Nano-Refrigerant, J. Mol. Liq. 365 (2022) 120125.